A continuous analytic channel potential solution to doped symmetric double-gate MOSFETs from the accumulation to the strong-inversion region*

He Jin(何 进)[a)b)c)†], Liu Feng(刘 峰)[c)], Zhou Xing-Ye(周幸叶)[c)], Zhang Jian(张 健)[c)], and Zhang Li-Ning(张立宁)[c)]

[a)] *School of Electronics and Information, Nantong University, Nantong* 226019, *China*

[b)] *The Key Laboratory of Integrated Microsystems, School of Computer & Information Engineering, Peking University Shenzhen Graduate School, Shenzhen* 518055, *China*

[c)] *TSRC, Institute of Microelectronics, School of Electronic Engineering and Computer Science, Peking University, Beijing* 100871, *China*

(Received 12 December 2009; revised manuscript received 6 February 2010)

A continuous yet analytic channel potential solution is proposed for doped symmetric double-gate (DG) MOSFETs from the accumulation to the strong-inversion region. Analytical channel potential relationship is derived from the complete 1-D Poisson equation physically, and the channel potential solution of the DG MOSFET is obtained analytically. The extensive comparisons between the presented solution and the numerical simulation illustrate that the solution is not only accurate and continuous in the whole operation regime of DG MOSFETs, but also valid to wide doping concentration and various geometrical sizes, without employing any fitting parameter.

Keywords: MOSFETs, transistors, doping, modeling, double-gate (DG)

PACS: 61.44.Br, 73.40.Ns, 73.40.Ty **DOI:** 10.1088/1674-1056/20/1/016102

1. Introduction

In order to extend CMOS scaling down to the performance limit, double-gate (DG) MOSFET is proposed as a promising non-classical structure to replace the traditional bulk CMOS devices.[1,2] Paralleling with the advance of fabrication technology and structure revolution,[3] device physics research[4] and compact model development of DG MOSFET also become intense subjects. The previous DG MOSFET compact models, however, were derived mainly from Poisson equation on the assumption that only the mobile charge was considered while the doping effect was neglected. As a result, the model applicability is limited to the undoped (lightly-doped) DG MOSFET case.[5−9] Moreover, most of these studies concerned only on the device operation region above the flat band although the supplied voltage could drive the transistor into accumulation region.[5−7] On the other hand, recent studies found that both the electron and hole played important roles simultaneously in the small bias voltage region, which did not only affect the model accuracy, more importantly, it also determined the global continuity from the accumulation to the strong inversion region.[9,10] However this important continuity issue, which is a key property of the device model for the circuit simulation and design,[11] has not been accounted for by most of the previous DG MOSFET compact models.

In the present work, a complete 1-D Poisson equation is addressed physically to obtain the continuous channel potential solution for symmetric DG MOSFET from the heavily doped body to the intrinsic channel. Extensive verifications for different operation regions, doping concentrations and geometrical sizes are carried out by comparison with the 2-D numerical simulation to illustrate the solution accuracy and continuity. Short channel effects and other advanced effects are further worked out within this modeling framework.

2. Model development

Figure 1 shows the schematic structure, coordinate system, and band diagram of an N-type symmetric DG MOSFET.

*Project supported by the National Natural Science Foundation of China (Grant No. 60876027), and the Open Funds of Jiangsu Province Key Lab of ASIC Design (JSICK1007).

†Corresponding author. E-mail: frankhe@ntu.edu.cn

© 2011 Chinese Physical Society and IOP Publishing Ltd

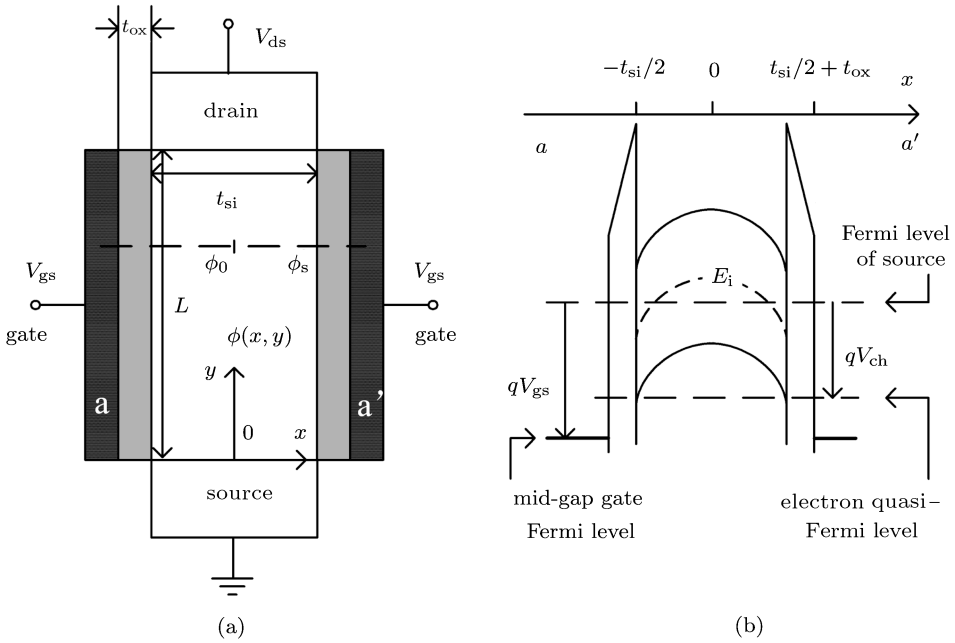


Fig. 1. (a) Schematic diagram and coordinate system of a doped symmetric DG MOSFET, and (b) corresponding energy band diagram along a vertical cut (aa') , where V_{ch} is the electron quasi-Fermi potential at a point in the channel with respect to the Fermi potential of the source, ϕ_s and ϕ_0 are the normalized channel potentials $\phi(x)$ at the silicon surface and centre.

Since the source is grounded, we regard its Fermi level as the energy reference. Two gates with the same mid-gap metal material and geometry parameters are tied to the same gate voltage V_{gs}. Under the gradual-channel approximation (GCA), the electrostatics in the silicon film of this DG MOSFET is described by a complete 1-D Poisson equation with the contributions of electrons, holes, acceptors, and donator charge:

$$\frac{\mathrm{d}^2\phi}{\mathrm{d}x^2} = \frac{qN_\mathrm{a}}{\varepsilon_\mathrm{si}\phi_\mathrm{t}}[\mathrm{e}^{\phi-2\phi_\mathrm{f}-v} - \mathrm{e}^{-\phi} + 1 - \mathrm{e}^{-2\phi_\mathrm{f}-v}], \quad (1)$$

where all potentials are normalized by the thermal voltage ϕ_t, i.e., v is the normalized V_{ch}, and $\phi_\mathrm{f} = \ln(N_\mathrm{a}/n_i)$ is the normalized Fermi potential of the silicon body with doping concentration N_a. All other symbols in this work take their usual meanings unless otherwise specified. The boundary conditions for Eq. (1) in the surface and the centre of the silicon film are written as

$$\left.\varepsilon_\mathrm{si}\frac{\mathrm{d}\phi}{\mathrm{d}x}\right|_{x=t_\mathrm{si}/2} = C_\mathrm{ox}(\nu_\mathrm{gs} - v_\mathrm{fb} - \phi_\mathrm{s}), \quad \text{and}$$
$$\left.\frac{\mathrm{d}\phi}{\mathrm{d}x}\right|_{x=0} = 0, \quad (2)$$

where ν_{gs} and v_{fb} are the normalized gate voltage and flat-band voltage respectively. Integrating $\mathrm{d}\phi$ in Eq. (1) and using boundary condition (2) result in the conventional DG MOSFET voltage equation with ϕ_s and ϕ_0:

$$\begin{aligned}(\nu_\mathrm{gs} - v_\mathrm{fb} - \phi_\mathrm{s})^2 = \gamma^2[&\mathrm{e}^{-2\phi_\mathrm{f}-v}(\mathrm{e}^{\phi_\mathrm{s}} - \mathrm{e}^{\phi_0}) \\ &+ \mathrm{e}^{-\phi_\mathrm{s}} - \mathrm{e}^{-\phi_0} + \phi_\mathrm{s} - \phi_0 \\ &- \mathrm{e}^{-2\phi_\mathrm{f}-v}(\phi_\mathrm{s} - \phi_0)], \end{aligned} \quad (3)$$

where $\gamma = \sqrt{2q\varepsilon_\mathrm{si}N_\mathrm{a}/\phi_\mathrm{t}C_\mathrm{ox}^2}$ is the bulk factor, normalized by $\sqrt{\phi_\mathrm{t}}$. In order to obtain the solutions of ϕ_s and ϕ_0, another equation is derived from Eq. (1) by integrating it twice along the coordinate position as

$$\begin{aligned}\phi(x) = \phi_0 + \frac{qN_\mathrm{a}}{\varepsilon_\mathrm{si}\phi_\mathrm{t}}\int_0^x\int_0^z [&\mathrm{e}^{\phi-2\phi_\mathrm{f}-v} - \mathrm{e}^{-\phi} \\ &+ 1 - \mathrm{e}^{-2\phi_\mathrm{f}-v}]\mathrm{d}y\mathrm{d}z, \\ &0 \le x \le z \le t_\mathrm{si}/2. \end{aligned} \quad (4)$$

Since this integral equation has the form $p = g(p)$, where $p = \phi$, its root can be approached by the sequence p_1, p_2,..., calculated by $p_{n+1} = g(p_n)$ staring from a fixed-point p_0 based on the fixed-point method in the numerical analysis.[12] In the present work, the fixed-point method is just repeated twice analytically to obtain a relation between ϕ_s and ϕ_0, staring from the local-approximation $\phi(x) = \phi_0$.[13] The following discussion will demonstrate that the result obtained by this approach is accurate enough to

predict the channel potential. Substituting the fixed-point $\phi(x) = \phi_0$ into the right hand side (RHS) of (4) yields the one-order solution of Eq. (4) as

$$\phi(x) \approx \phi_0 + h \cdot (2x/t_{\rm si})^2, \tag{5}$$

where

$$h(\phi_0) = \left(\frac{qN_{\rm a}t_{\rm si}^2}{8\varepsilon_{\rm si}\phi_{\rm t}}\right)[{\rm e}^{\phi_0 - 2\phi_{\rm f} - v} - {\rm e}^{-\phi_0} + 1 - {\rm e}^{-2\phi_{\rm f} - v}].$$

The final relation between $\phi_{\rm s}$ and ϕ_0 is obtained by substituting Eq. (5) in the RHS of Eq. (4) again, and evaluating the integral result in the silicon surface:

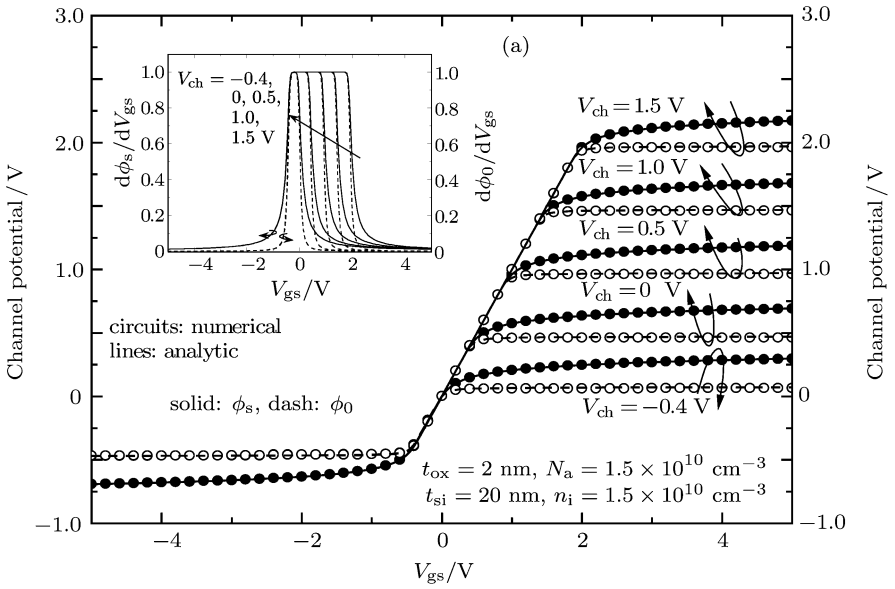
$$\begin{aligned}\phi_{\rm s} - \phi_0 = & \left(\frac{qN_{\rm a}t_{\rm si}^2}{8\varepsilon_{\rm si}\phi_{\rm t}}\right)[s_{\rm I} \cdot {\rm e}^{\phi_0 - 2\phi_{\rm f} - v} - s_{\rm A} \\ & \times {\rm e}^{-\phi_0} + 1 - {\rm e}^{-2\phi_{\rm f} - v}],\end{aligned} \tag{6}$$

where $s_{\rm I}(\phi_0) = (1 - {\rm e}^h)/h + \sqrt{\pi/h} \cdot {\rm erfi}[\sqrt{h}]$ and $s_{\rm A}(\phi_0) = ({\rm e}^{-h} - 1)/h + \sqrt{\pi/h} \cdot {\rm erf}[\sqrt{h}]$ when $\nu_{\rm gs}$ is above $v_{\rm fb}$; $s_{\rm I}(\phi_0) = (1 - {\rm e}^h)/h + \sqrt{-\pi/h} \cdot {\rm erf}[\sqrt{-h}]$ and $s_{\rm A}(\phi_0) = ({\rm e}^{-h} - 1)/h + \sqrt{-\pi/h} \cdot {\rm erfi}[\sqrt{-h}]$ when $\nu_{\rm gs}$ is below $v_{\rm fb}$. ${\rm erfi}[w]$ and ${\rm erf}[w]$ are the well-known imaginary error function and error function, respectively, and their polynomial approximations are introduced.[14]

By solving the equation group consisting of Eqs. (3) and (6), channel potentials $\phi_{\rm s}$ and ϕ_0 are obtained by Newton–Raphson (NR) method for given $V_{\rm gs}$ and $V_{\rm ch}$. In the present work, we use the continuous bulk surface potential solution[15] as the initial $\phi_{\rm s}$. From this initial guess, ϕ_0 and ${\rm d}\phi_0/{\rm d}\phi_{\rm s}$ are obtained from Eq. (6), and then an updated $\phi_{\rm s}$ is calculated by the NR method from Eq. (3). This loop continues until $\phi_{\rm s}$ converges to the required accuracy. Practical test shows that it requires 4 to 6 external iterations for $\phi_{\rm s}$ to reach a relative error 1‰, depending on the doping and biasing conditions.

3. Results and discussion

The solution predicted channel potentials for long-channel doped symmetric DG MOSFETs are illustrated in Fig. 2 for different operation regions and doping concentrations, compared with the 2-D numerical simulations.[14] It is evident that both $\phi_{\rm s}$ and ϕ_0 predicted by the presented solution show that they are in excellent agreement with the numerical simulations, from the accumulation, through the weak inversion, and finally to the strong-inversion regions. In addition, the solution continuity is demonstrated by plotting the potential derivative with respect to the gate voltage, which are shown in the insets of Fig. 2. It is observed that all the derivative curves show excellent continuity and smoothness in the whole operation regime.



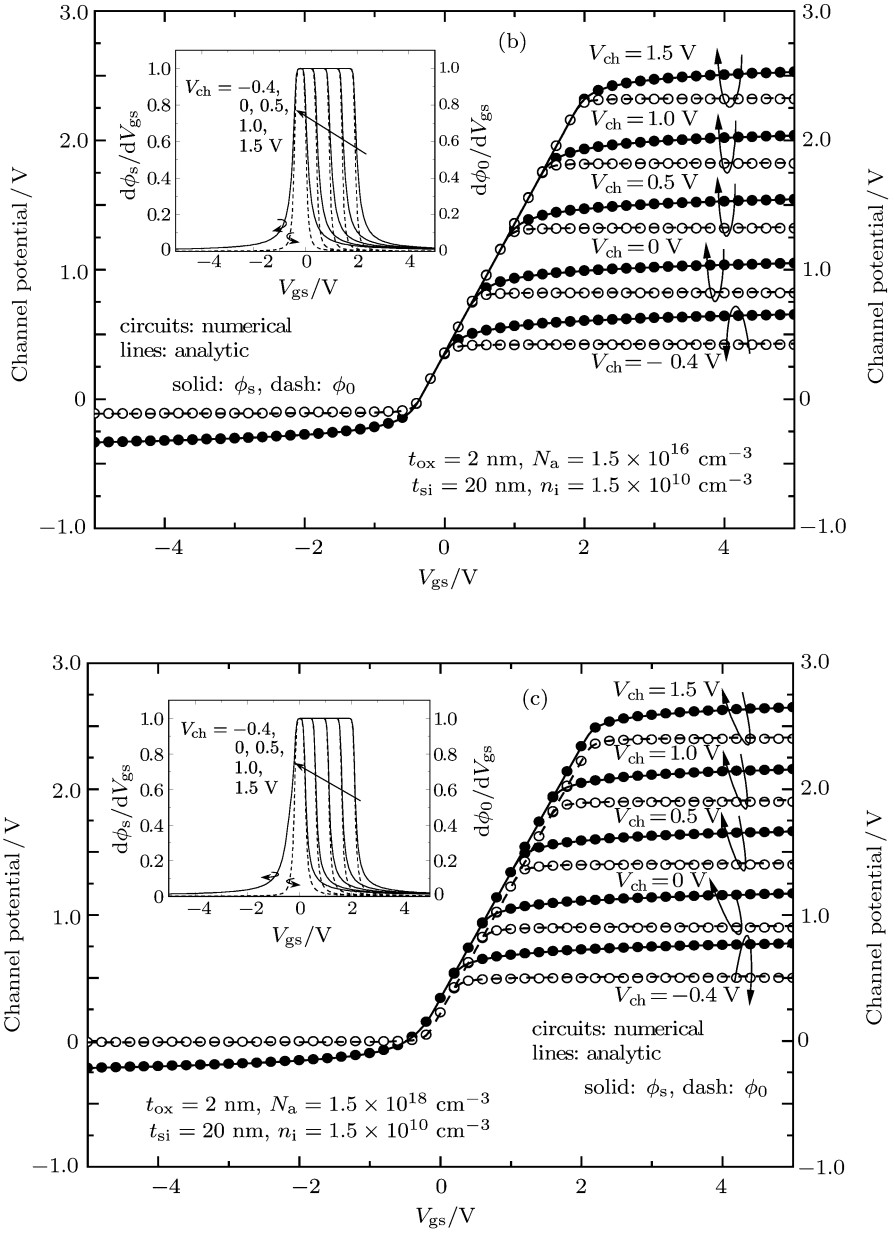


Fig. 2. Solution predicted channel potentials of symmetric DG MOSFETs with three typical doping concentrations: (a) intrinsic, (b) moderate doping, and (c) heavy doping. Different quasi-Fermi potentials are included in both analytic model and numerical simulations. Corresponding derivatives of the solution predicted channel potentials are shown in the insets.

The presented solution scaling abilities for different geometrical dimensions are demonstrated in Figs. 3 and 4 by the comparison between the solution prediction and 2-D numerical simulation for a heavily-doped and a moderately-doped DG MOSFET, respectively. In addition to the high accuracy and the smooth continuity of the predicted channel potential, the presented solution also captures the dynamic depletion behaviour, i.e., the heavily doped DG MOSFET operation transits from the partially-depleted to fully-depleted mode with the gate voltage increasing, without employing any fitting parameter.

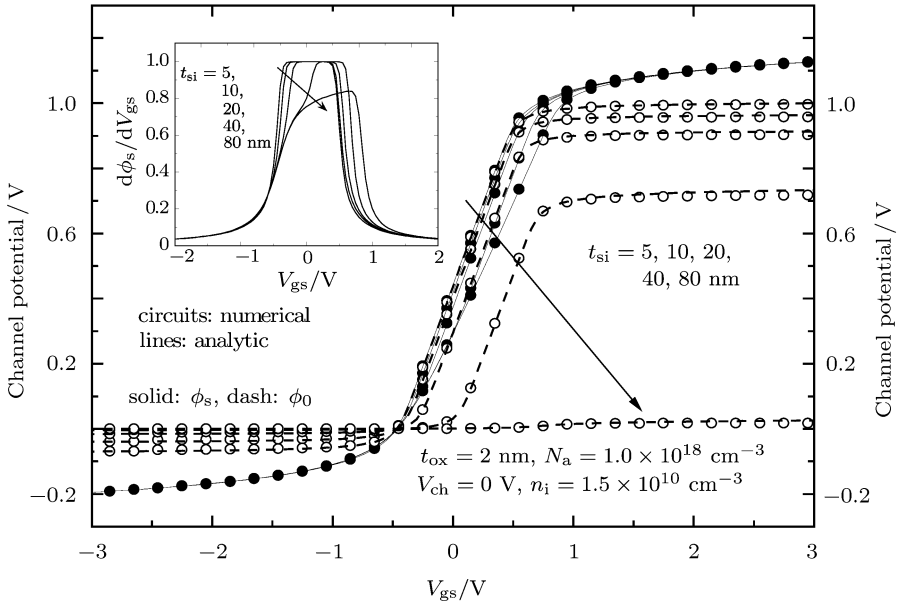


Fig. 3. Solution predicted channel potentials and their derivatives of doped symmetric DG MOSFETs with different silicon film thicknesses. Transition between the partially-depleted and the fully-depleted operation modes of a DG MOSFET with thick silicon film is predicted automatically.

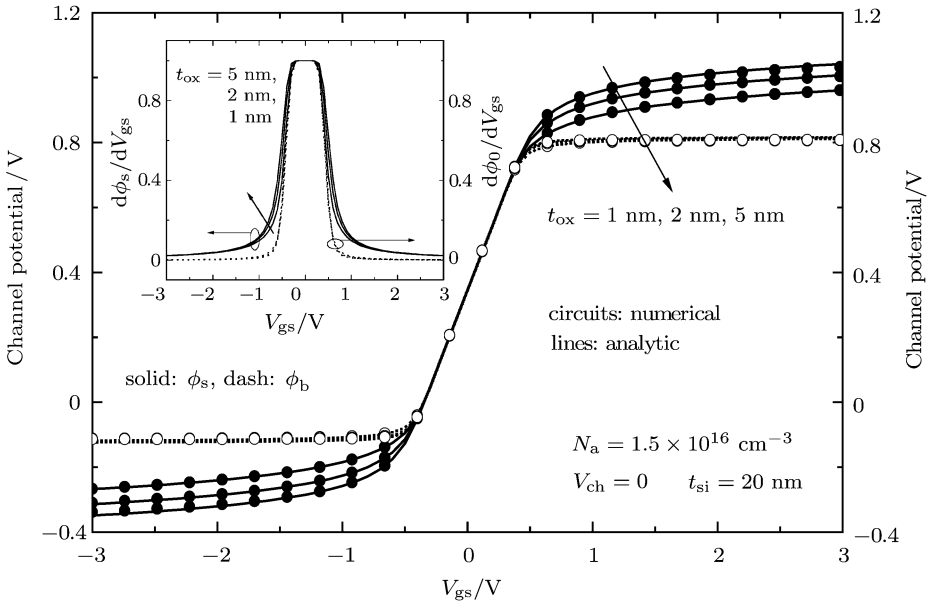


Fig. 4. Solution predicted channel potentials and their derivatives of moderately-doped symmetric DG MOSFETs with different gate oxide thicknesses. The inset shows the corresponding derivatives of channel potential versus gate voltage.

4. Conclusion

A continuous yet analytical channel potential solution from the accumulation to the strong inversion region is developed for the symmetric DG MOSFETs from the heavily doped body to the intrinsic channel. The solution predicted results are compared with the 2-D numerical simulations for different biasing conditions, doping concentrations and geometrical sizes. Excellent accuracy and continuity of the proposed solution are observed for the whole operation regime, without any fitting parameters. Short channel effects and other advanced effect models, which are ignored for the analysis simplicity here, will be added in the future work.

References

[1] Frank D J, Laux S E and Fischetti M V 1992 *IEDM Tech. Dig.* p553

[2] Chen Q, Bowman K A, Harrell E M and Meindl J D 2003 *IEEE Circuits Devices Mag.* **19** 28

[3] Balestra F and Jomaah J 2005 *Microelectronic Engineering* **80** 230

[4] Xia Y W and Wang S W 1990 *Chin. J. Semiconductors* **11** 962

[5] Taur Y 2000 *IEEE Electron Device Lett.* **21** 245

[6] Sallese J M, Krummenacher F, Pregaldiny F, Lallement C, Roy A S and Enz C C 2005 *Solid-State Electron.* **49** 485

[7] Adelmo Ortiz-Conde, Francisco J García-Sánchez and Slavica Malobabic 2005 *IEEE Trans. Electron Devices* **52** 1669

[8] He J, Liu F, Zhang J, Feng J, Hu J H, Yang S Q and Chan M S 2007 *IEEE Trans. Electron Devices* **54** 1203

[9] Zhou X, Zhu Z M, Rustagi S C, See G H, Zhu G J, Lin S H, Wei C Q and Lim G H 2008 *IEEE Trans. Electron Devices* **55** 616

[10] He J, Chen Y, Li B, Wei Y Q and Chan M S 2008 *Workshop on Compact Modeling, NSTI-Nanotech*

[11] Compact Model Council Homepage. [Online]. Available: www.eigroup.org/cmc

[12] Conte S D and de Boor C 1980 *Elementary Numerical Analysis: An Algorithmic Approach* (McGraw-Hill) p56

[13] Francis P, Terao A, Flandre D and van de Wiele F 1995 *Solid-State Electron.* **38** 171

[14] http://mathworld.wolfram.com.

[15] He J, Chan M S, Zhang X and Wang Y Y 2006 *IEEE Trans. Electron Devices* **53** 2008